Theoretical Study of Two-Photon Absorption Properties of a Series of Ferrocene-Based Chromophores

Xiang-Biao Zhang,[†] Ji-Kang Feng,*[,†,‡] Ai-Min Ren,[†] and Chia-Chung Sun[†]
State Key Laboratory of Theoretical and Computational Chemistry, Institute of Theoretical Chemistry, and College of Chemistry, Jilin University, Changchun, 130023, China
Received: April 16, 2006; In Final Form: July 21, 2006

The electronic structures, one-photon absorption (OPA), and two-photon absorption (TPA) properties of a series of ferrocene-based chromophores with TCF-type acceptors (TCF = 2-dicyanomethylene-3-cyano-4-methyl-2,5-dihydrofuran) have been studied by using the ZINDO−SOS method. The results have revealed that OPA and TPA of ferrocenyl derivatives are affected by the strength of the acceptor, especially the π-bridge conjugation length. The TPA cross section increases with increasing acceptor strength and π-bridge conjugation length. The TCF-type acceptor with a phenyl group can lead to a larger TPA cross section. Quadrupole molecules have the largest TPA cross sections (2000−3000 GM), which are about 4 times that of the corresponding dipolar molecules, indicating larger interactions between the top and bottom branches. Finally, the origins of the two-photon excitations for ferrocenyl derivatives are analyzed. The calculations show that ferrocenyl derivatives with TCF-type acceptors (especially quadrupole molecules) are promising candidates for TPA materials.

1. Introduction

There is significant interest in the development of two-photon absorption (TPA) materials because of their potential applications such as upconverted lasing,[1−3] optical power limiting,[4−6] photodynamic therapy,[7] and three-dimensional (3D) microfabrication.[8−10] Extensive studies have been conducted, and great progress has been made on the relationship between molecular structure and TPA cross section.[11−21] Some basic structural motifs have been revealed to be important regarding TPA molecular construction. Molecular structures containing a π-center with electron donors or acceptors on the terminal sites of the conjugation system are expected to exhibit good TPA response. Particularly, the conjugation length, π-electron center, and chemical functional groups at the end of electron conjugation are recognized as three important factors for structure−property optimization.[11,12,14,15] Much work has focused on linear quadrupole molecules as potential TPA dyes.[11,22] Another strategy toward the enhancement of TPA beyond linear chromophores has been the development of multibranched[17,23,24] and/or dendritic chromophores[25−28] where collections of TPA active subunits extend into two or three dimensions. Prasad and co-workers showed that the multibranched structure significantly increases the TPA cross section in comparison to the one-branched counterparts.[17] Minhaeng Cho et al. investigated the TPA properties of a series of octupolar molecules and pointed out that for this kind of molecule the TPA cross section increases as the strength of the donor or acceptor increases and the TPA cross section is linearly proportional to the first hyperpolarizability.[29] Sahraoui and co-workers measured the third-order susceptibilities and TPAs in branched oligothienylenvinylene derivatives using a degenerate four-wave mixing technique.[30] They demonstrated that the values of third-order susceptibilities and TPA coefficients β increase as the number of branches increases.

Organometallic compounds are intriguing candidates for nonlinear optical (NLO) materials,[31−33] because (1) these compounds can have metal-to-ligand (MLCT) or ligand-to-metal (LMCT) charge-transfer bands, which are often associated with larger optical nonlinearities, in the UV−visible region of the spectrum; (2) coordinating a ligand containing highly polarizable π-electrons to a metallic center having weakly bound valence electrons (i.e., which is highly polarizable) could, in principle, yield electronic structures that exhibit enhanced optical nonlinearities; and (3) organometallic subunits, by virtue of the large number of available coordination sites about a metal center, could conceivably be incorporated into macroscopic matrixes through a variety of novel attachment schemes. Sandwich-type compounds, like ferrocene, are examples of organometallic systems of potential interest, because they contain aromatic cyclopentadienyl rings interacting with a metal atom through their π-electron systerms. Second-order and third-order nonlinear optical chromophores based on ferrocene are currently attracting a great deal of attention.[34−42] Ferrocene derivatives with $\mu\beta$ as large as $11\,200 \times 10^{-48}$ esu, comparable with the best all-organic chromophores, have been achieved.[43] Ghosal et al. investigated nonlinear properties of various aryl and vinyl derivatives of ferrocene by using the degenerate four-wave mixing technique.[34] Kanis et al. studied the second-order nonlinear optical responses of *trans*-1-ferrocenyl-2-(*N*-methylpyridinium-4-yl)ethylene iodide and *cis*-1-ferrocenyl-2-(4-nitrophenyl)ethylene using ZINDO combined with sum-over-states and gave results in accord with experimental values.[35] They pointed out that the molecular second hyperpolarizability increases strongly with the length of the conjugated π-electron systems and intense MLCT transitions dominate the optical nonlinearity, while the lower-frequency ligand-field-based excitations contribute little. Wright et al. studied second harmonic generation of main-chain, side-chain, and guest−host polymers of ferrocenyl chromophores.[44] A second harmonic intensity 4 times that of *y*-cut quartz crystal was measured. Some ferrocenyl complexes have been synthesized by Li et al., and the studied

* Corresponding author. Tel.: +864318499856. Fax: +864318945942. E-mail: jikangf@yahoo.com.
[†] Institute of Theoretical Chemistry.
[‡] Jilin University.

10.1021/jp062350z CCC: $33.50
Published on Web 10/13/2006

results show that these complexes possess larger second hyperpolarizability.[40] Liao et al. systematically studied a series of NLO chromophores incorporating the ferrocenyl group as an electron donor and dicyanomethylene-3-cyano-4- methyl-2,5-dihydrofuran derivatives as electron acceptors and pointed out that the first hyperpolarizabilities of ferrocenyl derivatives increase with the strengths of acceptors and the conjugation chain length and a linear relation exists between the hyperpolarizability and the bond length alternation.[42] Though TPA belongs to a third-order nonlinear optical phenomenon, the reports on TPA properties of ferrocene-containing chromophores are rare. In this paper, a series of ferrocenyl derivatives are designed, and their electronic structures and one- and two-photon absorption properties are studied.

2. Computational Methods

The TPA process corresponds to simultaneous absorption of two photons. The TPA efficiency of an organic molecule, at optical frequency $\omega/2\pi$, can be characterized by the TPA cross section $\delta(\omega)$. It can be directly related to the imaginary part of the second hyperpolarizability $\gamma(-\omega; \omega, \omega, -\omega)$ by ref 45

$$\delta(\omega) = \frac{3\hbar\omega^2}{2n^2c^2\epsilon_0} L^4 \,\mathrm{Im}[\gamma(-\omega; \omega, -\omega, \omega)] \qquad (1)$$

where $\hbar\omega$ is the energy of the incoming photons, c the speed of light, and ϵ_0 the vacuum electric permittivity. n denotes the refractive index of the medium, and L corresponds to the local-field factor. In the calculations presented here, n and L are set to 1 (isolated molecule in a vacuum).

The sum-over-states (SOS) expression to evaluate the components of the second hyperpolarizability $\gamma_{\alpha\beta\gamma\delta}$ can be deduced using perturbation theory and the density matrix method. By considering a Taylor expansion of energy with respect to the applied field, the $\gamma_{\alpha\beta\gamma\delta}$ Cartesian components are given by refs 46 and 47.

$$\begin{aligned}\gamma_{\alpha\beta\gamma\delta}(-\omega_\sigma; \omega_1, \omega_2, \omega_3) = \hbar^{-3}\sum P_{1,2,3}\Bigg(&\sum_{\mathrm{K}}{}'\sum_{L}{}'\sum_{\mathrm{M}}{}' \times \\ &\Bigg(\frac{\langle 0|\mu_\alpha|\mathrm{K}\rangle\langle \mathrm{K}|\overline{\mu_\beta}|L\rangle\langle L|\overline{\mu_\gamma}|\mathrm{M}\rangle\langle \mathrm{M}|\mu_\delta|0\rangle}{(\omega_{\mathrm{K}} - i\Gamma_{\mathrm{K}}/2 - \omega_\sigma)(\omega_L - i\Gamma_L/2 - \omega_2 - \omega_3)(\omega_{\mathrm{M}} - i\Gamma_{\mathrm{M}}/2 - \omega_3)} + \\ &\frac{\langle 0|\mu_\beta|\mathrm{K}\rangle\langle \mathrm{K}|\overline{\mu_\alpha}|L\rangle\langle L|\overline{\mu_\gamma}|\mathrm{M}\rangle\langle \mathrm{M}|\mu_\delta|0\rangle}{(\omega_{\mathrm{K}} + i\Gamma_{\mathrm{K}}/2 + \omega_1)(\omega_L - i\Gamma_L/2 - \omega_2 - \omega_3)(\omega_{\mathrm{M}} - i\Gamma_{\mathrm{M}}/2 - \omega_3)} + \\ &\frac{\langle 0|\mu_\beta|\mathrm{K}\rangle\langle \mathrm{K}|\overline{\mu_\gamma}|L\rangle\langle L|\overline{\mu_\alpha}|\mathrm{M}\rangle\langle \mathrm{M}|\mu_\delta|0\rangle}{(\omega_{\mathrm{K}} + i\Gamma_{\mathrm{K}}/2 + \omega_1)(\omega_L + i\Gamma_L/2 + \omega_1 + \omega_2)(\omega_{\mathrm{M}} - i\Gamma_{\mathrm{M}}/2 - \omega_3)} + \\ &\frac{\langle 0|\mu_\beta|\mathrm{K}\rangle\langle \mathrm{K}|\overline{\mu_\gamma}|L\rangle\langle L|\overline{\mu_\delta}|\mathrm{M}\rangle\langle \mathrm{M}|\mu_\alpha|0\rangle}{(\omega_{\mathrm{K}} + i\Gamma_{\mathrm{K}}/2 + \omega_1)(\omega_L + i\Gamma_L/2 + \omega_1 + \omega_2)(\omega_{\mathrm{M}} + i\Gamma_{\mathrm{M}}/2 + \omega_\sigma)}\Bigg) - \\ &\sum_{\mathrm{K}}{}'\sum_{L}{}'\Bigg(\frac{\langle 0|\mu_\alpha|\mathrm{K}\rangle\langle \mathrm{K}|\mu_\beta|0\rangle\langle 0|\mu_\gamma|L\rangle\langle L|\mu_\delta|0\rangle}{(\omega_{\mathrm{K}} - i\Gamma_{\mathrm{K}}/2 - \omega_\sigma)(\omega_{\mathrm{K}} - i\Gamma_{\mathrm{K}}/2 - \omega_1)(\omega_L - i\Gamma_L/2 - \omega_3)} + \\ &\frac{\langle 0|\mu_\alpha|\mathrm{K}\rangle\langle \mathrm{K}|\mu_\beta|0\rangle\langle 0|\mu_\gamma|L\rangle\langle L|\mu_\delta|0\rangle}{(\omega_{\mathrm{K}} - i\Gamma_{\mathrm{K}}/2 - \omega_1)(\omega_L + i\Gamma_L/2 + \omega_2)(\omega_L - i\Gamma_L/2 - \omega_3)} + \\ &\frac{\langle 0|\mu_\beta|\mathrm{K}\rangle\langle \mathrm{K}|\mu_\alpha|0\rangle\langle 0|\mu_\gamma|L\rangle\langle L|\mu_\delta|0\rangle}{(\omega_{\mathrm{K}} + i\Gamma_{\mathrm{K}}/2 + \omega_1)(\omega_{\mathrm{K}} + i\Gamma_{\mathrm{K}}/2 + \omega_\sigma)(\omega_L + i\Gamma_L/2 + \omega_2)} + \\ &\frac{\langle 0|\mu_\beta|\mathrm{K}\rangle\langle \mathrm{K}|\mu_\alpha|0\rangle\langle 0|\mu_\gamma|L\rangle\langle L|\mu_\delta|0\rangle}{(\omega_{\mathrm{K}} + i\Gamma_{\mathrm{K}}/2 + \omega_1)(\omega_L + i\Gamma_L/2 + \omega_2)(\omega_L - i\Gamma_L/2 - \omega_3)}\Bigg)\Bigg) \qquad (2)\end{aligned}$$

In this formula, α, β, γ, and δ refer to the molecular axes; ω_1, ω_2, and ω_3 are optical frequencies, and $\omega_\sigma = \omega_1 + \omega_2 + \omega_3$ is the polarization response frequency; $\sum P_{1,2,3}$ indicates a sum over the terms obtained by the six permutations of the pairs (ω_1/μ_β), (ω_2/μ_γ), and (ω_3/μ_δ); K, L, and M denote excited states and 0 the ground state; $|\mathrm{K}\rangle$ is an electronic wave function with energy $\hbar\omega_{\mathrm{K}}$ relative to the ground electronic state; μ_α is the α_{th} ($= x, y, z$) component of the dipole operator, $\langle \mathrm{K}|\overline{\mu_\alpha}|L\rangle = \langle \mathrm{K}|\mu_\alpha|L\rangle - \langle 0|\mu_\alpha|0\rangle\delta_{KL}$; the primes on the summation over the electronic states indicate exclusion of the ground state. Γ_{K} is the damping factor of excited-state K, and in the present work, all damping factors Γ are set to 0.14 eV. To compare the calculated δ value with the experimental value measured in solution, the orientationally averaged (isotropic) value of γ is evaluated, which is defined as

$$\langle\gamma\rangle = \frac{1}{15}\sum_{i,j}(\gamma_{iijj} + \gamma_{ijij} + \gamma_{ijji}) \quad i, j = x, y, z \qquad (3)$$

Substituted the imaginary part of the $\langle\gamma\rangle$ value into eq 1, $\delta(\omega)$ that can be compared with the experimental value is obtained.

Generally, the position and relative strength of the two-photon response are to be predicted using the following simplified form of the SOS expression (three-state formula):[48]

$$\delta \propto \frac{\mathrm{M}_{0k}{}^2\mathrm{M}_{kn}{}^2}{(\mathrm{E}_{0k} - \mathrm{E}_{0n}/2)^2\Gamma} + \frac{\mathrm{M}_{0n}{}^2\Delta\mu_{0n}{}^2}{(\mathrm{E}_{0n}/2)^2\Gamma} \qquad (4)$$

where M_{0k}, M_{0n}, and M_{kn} denote the transition dipole moments from states 0 to k, 0 to n, as well as k to n, respectively; E_{0k} and E_{0n} denote the excitation energies from states 0 to k as well as 0 to n, respectively; the subscripts 0, k, and n refer to the ground state S_0, the intermediate state S_k, and the TPA final state S_n, respectively; and $\Delta\mu_{0n}$ is the dipole moment difference between S_0 and S_n.

In principle, any kind of self-consistent-field molecular orbital procedure combined with configuration interaction (CI) can be used to calculate the physical values in the above expressions. In this paper, the DFT/B3LYP/6-31G method was first used to calculate molecular equilibrium geometries. Then, the properties of electronic excited states were obtained by single and double electronic excitation configuration interaction (SDCI) using the ZINDO program.[49] For all the molecules studied here, the CI-active spaces were restricted to the 40 highest occupied and 40 lowest unoccupied π-orbitals for singly excited configuration and to the 3 highest occupied and 3 lowest unoccupied π-orbitals for doubly excited configuration. Furthermore, one-photon absorption (OPA) parameters that are needed to predict TPA properties were provided. Then, according to the formula (eqs 1−3), the second hyperpolarizabilities γ and the TPA cross sections $\delta(\omega)$ have been calculated. The calculated TPA cross sections of every molecule include the contributions from 300 lowest-lying excited states. A chosen basis set size of 300 states included in both configuration interaction and SOS expansion is sufficient for convergence for $\delta(\omega)$ of all the molecules (see Supporting Information).

3. Results and Discussions

3.1. Molecular Design and Optimization. The chemical structures of studied molecules are displayed in Figure 1. The 2-dicyanomethylene-3-cyano-4-methyl-2,5-dihydrofuran (TCF)-type acceptors are stronger and possess peculiar characteristics,[42] providing a new strategy to develop better NLO materials and help us to understand the effects of acceptors and π-conjugated chains on NLO of materials. In our paper, the methyl groups in TCF are substituted with CF_3, CN, and phenyl (Ph) groups, forming acceptors CF_3PhTCF, CNPhTCF, and CNCNTCF. The

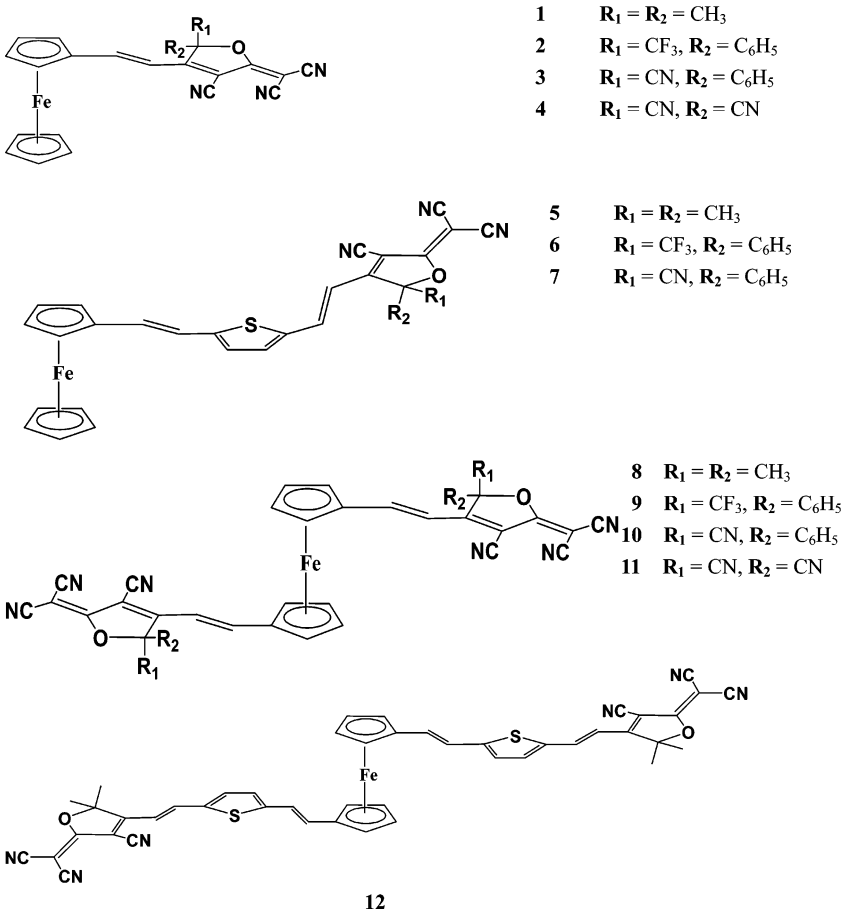

Figure 1. Chemical structures of studied molecules.

strengths of these acceptors are in the order of TCF < CF_3-PhTCF ≈ CNPhTCF < CNCNTCF. As shown in Figure 1, the studied molecules can be divided into two groups. One is D (donor)-π-A (acceptor) type dipolar molecules such as **1**−**7**, and another is A-π-D-π-A type quadrupole molecules such as **8**−**12**. The molecules **1**−**4** and **8**−**11** with the ferrocenyl (Fc) group as an electron donor and TCF, CF_3PhTCF, CNPhTCF, and CNCNTCF as electron acceptors provide a possibility of assessing the effects of the strengths of acceptors on the TPA of a material. To further ascertain the effects of increasing π-bridge length conjugation on the TPA of a material, the molecules **5**−**7** and **12** have been built by inserting a vinyl-thiophen chain between donor and acceptor groups of **1**−**4** and **8**. All the molecular geometries have been calculated with the hybrid B3LYP functional combined with the 6-31G basis set using the *Gaussian 03* program suite.[50] To compare the optimized results with the experimental data, the Supporting Information collects the selected bond lengths for the ferrocenyl segments in the optimized geometries of the molecules **1**, **2**, **5**, and **6**, as well as the corresponding single-crystal X-ray diffraction data. Our calculated bond lengths are in agreement with the single-crystal X-ray diffraction data; the maximum error is smaller than 0.06 Å. At the B3LYP/6-31G level, the ferrocenyl group in the molecule takes an eclipsed conformation; the average Fe−C_{ring} distance is about 2.082 Å, the average intra C−C bond length and C−C−C angle of cyclopentadienyl (Cp) are 1.437 Å and 107.99°, respectively, which are slightly larger than 2.04 Å, 1.416 Å, and 107.8° reported in the literature.[40] The two Cp rings in the ferrocenyl group are perfectly planar and nearly parallel. The deviations between the Cp and the vinyl plane connected to it are in the range 3.89−12.73°; molecules **1** and **8** with the relatively weak acceptor TCF have the smallest deviations of 6.23° and 3.89°, respectively, while molecules **4** and **11** with the strongest acceptor CNCNTCF have the largest deviations of 11.28° and 12.73°, respectively. The other parts in the studied molecules are in the same plane except for the substituents appended to the acceptors.

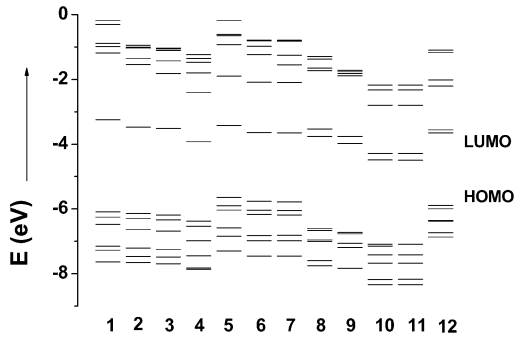

Figure 2. B3LYP/6-31G predicted molecular orbital energy diagram.

3.2. Electronic Structures and One-Photon Absorptions. The frontier orbital energies predicted with the B3LYP/6-31G method are schematically plotted in Figure 2. The energies of the highest occupied molecular orbital (HOMO), the lowest unoccupied molecular orbital (LUMO), HOMO − *n*, and LUMO + *n* (*n* = 1, 2, and 3) are summarized in Table 1. From Figure 2 and Table 1, some characteristics of the electronic structures of ferrocenyl derivatives can be found: (1) As the strengths of the acceptors increase (TCF < CF_3PhTCF ≈ CNPhTCF < CNCNTCF), the HOMO and LUMO energy levels decrease. (2) With increasing the π-bridge conjugation length, the HOMO energies increase and the LUMO energies decrease

TABLE 1: Energies of the Frontier Molecular Orbitals HOMO − *n* and LUMO + *n* (*n* = 0, 1, 2, and 3)[a]

mol	1	2	3	4	5	6	7	8	9	10	11	12
HOMO − 3	−7.149	−7.206	−7.250	−7.445	−6.582	−6.820	−6.814	−6.998	−7.187	−7.673	−7.673	−6.378
HOMO − 2	−6.477	−6.630	−6.682	−6.986	−6.035	−6.165	−6.181	−6.955	−7.060	−7.415	−7.415	−6.349
HOMO − 1	−6.252	−6.291	−6.338	−6.536	−5.905	−6.038	−6.046	−6.662	−6.767	−7.148	−7.148	−5.993
HOMO	−6.085	−6.138	−6.187	−6.378	−5.645	−5.762	−5.782	−6.599	−6.725	−7.087	−7.087	−5.894
LUMO	−3.244	−3.474	−3.518	−3.922	−3.424	−3.641	−3.650	−3.757	−3.981	−4.489	−4.489	−3.648
LUMO + 1	−1.184	−1.539	−1.818	−2.408	−1.903	−2.084	−2.095	−3.526	−3.763	−4.286	−4.286	−3.561
LUMO + 2	−0.986	−1.349	−1.428	−1.798	−0.927	−1.231	−1.547	−1.731	−1.891	−2.799	−2.799	−2.207
LUMO + 3	−0.885	−1.033	−1.105	−1.467	−0.652	−0.978	−1.261	−1.652	−1.820	−2.796	−2.796	−2.017

[a] Unit: eV.

TABLE 2: OPA Properties for Studied Molecules

	lowest energy transition		higher energy transition		
mol	λ^{O}_{max}/nm	oscillator strength (*f*)	λ^{O}_{max}/nm	oscillator strength (*f*)	CI coefficient
1	671.7 (630)[42]	0.011	449.5 (424)[42]	0.781	0.88(H → L)
2	678.6 (684)[42]	0.011	450.1 (442)[42]	0.831	0.89(H → L)
3	680.4	0.012	448.9	0.831	0.89(H → L)
4	695.1	0.020	466.1	0.747	0.87(H → L)
5	649.0 (664)[42]	0.016	524.3 (522)[42]	1.180	−0.94(H → L)
6	653.2 (738)[42]	0.029	551.4 (562)[42]	1.255	0.93(H → L)
7	654.1	0.028	550.1	1.267	0.93(H → L)
8	646.8	0.013	432.2	1.582	−0.39(H−1 → L) − 0.55(H−1 → L+1) + 0.58(H → L)
9	638.8	0.016	431.5	1.652	0.58(H−1 → L+1) + 0.61(H → L)
10	640.2	0.014	430.4	1.733	−0.61(H−1 → L+1) − 0.62(H → L)
11	661.4	0.016	440.7	1.780	−0.68(H−1 → L+1) + 0.62(H → L)
12	644.3	0.031	519.6	2.083	0.36(H−1 → L) − 0.46(H−1 → L+1) + 0.45(H → L) + 0.57(H → L+1)

(from **1** to **5**, **2** to **6**, and **3** to **7**). However, there is an exception in which the LUMO energy of **8** is −3.76 eV smaller than that of **12** (−3.65 eV). (3) In comparison with the dipolar molecules, the energy levels of HOMO and LUMO for the quadrupole molecules are lower. (4) The HOMO−LUMO energy gaps change in the order of **1** (2.84 eV) = **8** (2.84 eV) > **9** (2.74 eV) > **3** (2.67 eV) > **2** (2.66 eV) > **10** (2.60 eV) = **11** (2.60 eV) > **4** (2.46 eV) > **12** (2.26 eV) > **5** (2.22 eV) > **7** (2.13 eV) > **6** (2.12 eV). Comparing the HOMO−LUMO energy gaps of these molecules, we find that the HOMO−LUMO energy gaps reduce as the π-bridge conjugation length increases, and the effects of the π-bridge conjugation length on the HOMO−LUMO energy gaps are larger than that of the acceptors. A marked feature of the energy diagram is the large energy gaps between the LUMO and LUMO + 1 for the dipolar molecules **1**−**7** as well as between the LUMO + 1 and LUMO + 2 for the quadrupole molecules **8**−**12**. The LUMO−LUMO + 1energy gaps of **1**−**4** are in the range 1.51−2.06 eV, the LUMO−LUMO + 1 energy gaps of **5** and **6** are about 1.56 eV, and in the quadrupolar molecules **8**−**12**, the LUMO−LUMO + 1 energy gaps decrease to about 0.20 eV.

The OPA spectra of studied molecules have been calculated by the ZINDO method. The maximum OPA wavelengths (λ^{O}_{max}), the corresponding oscillator strengths (*f*), and the transition natures are tabulated in Table 2. The theoretical and experimental data[42] for these molecules show two optical transitions. Note that the ZINDO-derived lowest-energy "transitions" for all structures possess very small oscillator strengths (0.011−0.031) relative to those of the higher-energy transitions (0.747−2.083). When the computed optical properties are compared with those from experiment, it can be seen that the ZINDO method successfully predicts the intense shorter-wavelength transitions. Though the ZINDO method less accurately predicts the characteristics of the weak longer-wavelength optical absorptions, it does not influence the accurate prediction of the TPA properties of ferrocenyl derivatives, because the longer-wavelength transitions contribute little to the NLO properties.[34,35] It can be found from Table 2 that, from 449.5 nm for **1** to 466.1 for **4**, the higher-energy absorption is red-shifted by 16.6 nm; from 524.3 nm for **5** to 550.1 nm for **7** and from 432.2 nm for **8** to 440.7 nm for **11**, the higher-energy absorptions are red-shifted by 25.8 and 8.5 nm, respectively. Therefore, as the strengths of acceptors increase from TCP to CNCNTCF, the higher-energy absorptions show red shifts (10−30 nm). When increasing the π-bridge conjugation length, the higher-energy absorptions are red-shifted by 75−100 nm from **1**−**3** and **8** to **5**−**7** and **12**. In comparison with **1**−**3**, the higher-energy absorptions of the quadrupole molecules **8**−**11** are blue-shifted by 17−26 nm (449.5, 450.1, 448.9, and 466.1 nm for **1**−**4**; 432.2, 431.5, 430.4, and 440.7 nm for **8**−**11**, respectively) and the oscillator strengths are increased by about two times. As shown in Table 2, the single electron excitation from HOMO to LUMO dominates the higher-energy transitions for the dipolar molecules **1**−**7**, while for the quadrupole molecules **8**−**12**, the single electron excitations between HOMO − 1, HOMO, LUMO, and LUMO + 1 have dominant contributions to the higher-energy transitions. This can be explained in terms of the structures of the energy level of molecule. There are far smaller energy gaps between HOMO and HOMO − 1 and between LUMO and LUMO + 1 in the quadrupole molecules **8**−**12** than in the dipolar molecules **1**−**7** (see Figure 2). The molecular orbital can be described as the linear combination of atomic orbitals (LCAO). Taking **1** as an example, we will analyze the nature of the higher-energy absorptions of ferrocenyl derivatives. Within the zero differential overlap (ZDO) approximation, the wave functions of HOMO and LUMO (Ψ^1_{HOMO} and Ψ^1_{LUMO}) of **1** are described as follows: $\Psi^1_{HOMO} = 0.30\Phi^1_{Fe}[3d(x^2 - y^2)] - 0.30\Phi^7_C[2p(z)] - 0.27\Phi^9_C[2p(z)]$, $\Psi^1_{LUMO} = -0.51\Phi^5_C[2p(z)] + 0.47\Phi^9_C[2p(z)] + 0.33\Phi^4_C[2p(z)]$. Here, $\Phi^n_A[b]$ denotes the wave function of the orbital *b* in atom *A*(*n*). In molecule **1**, atom Fe (1) locates in the center of the ferrocenyl group, and C(7) and C(9) are in the π-conjugation bridge, while atoms C(4) and C(5) locate in the acceptor. Apparently, the higher-energy absorption of **1** comes from the metal-to-ligand transition (MLCT). For other ferrocenyl derivatives, we can obtain the

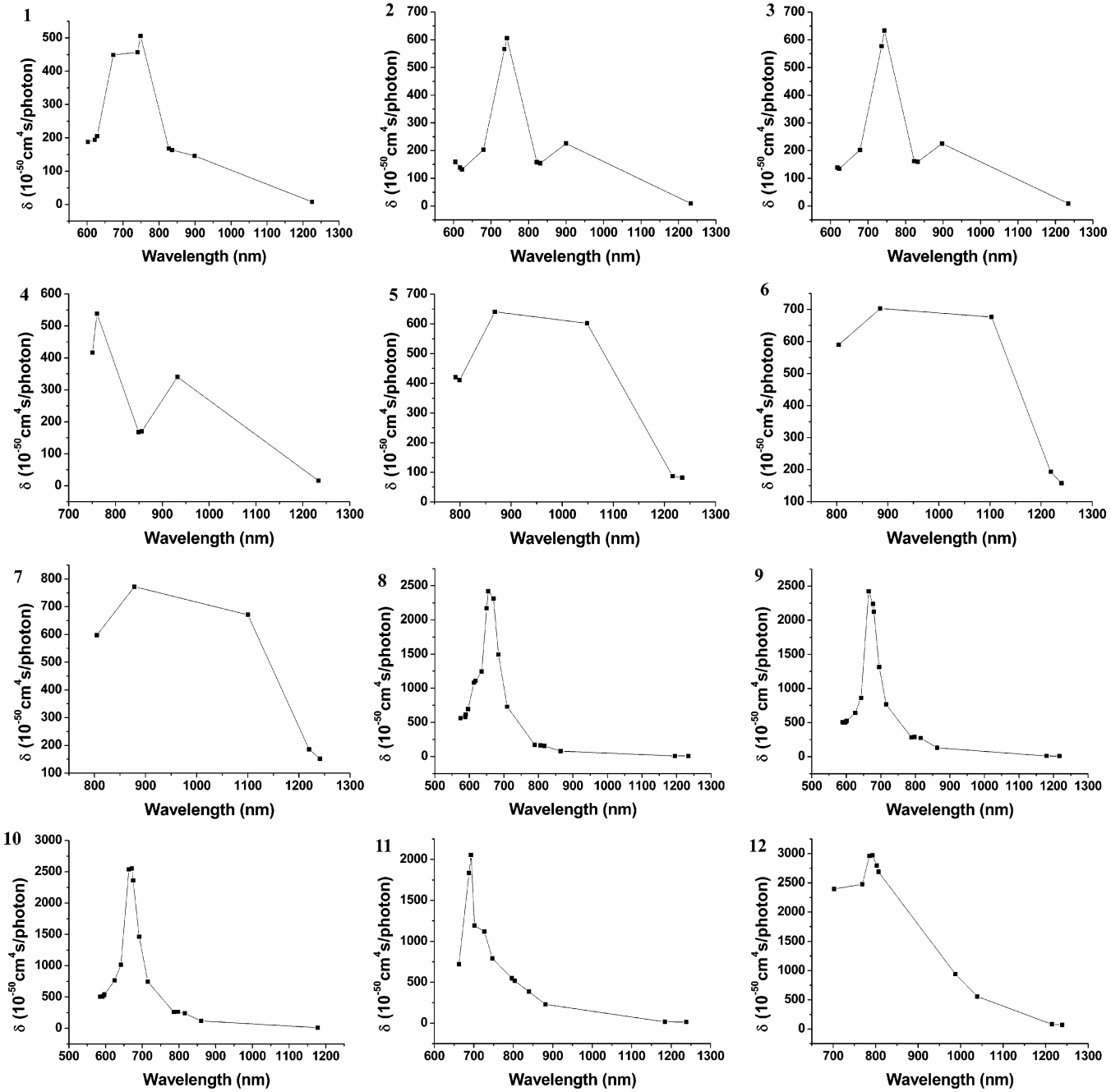

Figure 3. TPA spectra for studied compounds.

same conclusion. Contour surfaces of the frontier orbitals relevant to OPA are plotted in Figure 2 in the Supporting Information. We can clearly find that the HOMOs in **1**−**12** and (HOMO − 1)s in **8**−**12** are mainly distributed on the ferrocenyl moiety with some contribution from the π-bridge, while the LUMOs in **1**−**12** and (LUMO + 1)s in **8**−**12** are largely localized on the acceptors with some contribution from the π-bridge. Therefore, the higher-energy absorptions of the ferrocenyl derivatives (**1**−**12**) originate from charge transitions from the ferrocenyl moiety to the acceptor moiety (MLCT).

3.2. Two-Photon Absorptions. According to the expressions (eqs 2 and 3), the third-order nonlinear susceptibilities $\langle\gamma\rangle$ of the studied molecules have been calculated, and then TPA cross sections $\delta(\omega)$ have been obtained by using eq 1. The calculated results are summarized in Figure 3. The maximum TPA wavelengths (λ_{max}^{T}), the maximum TPA cross sections (δ_{max}^{T}), the imaginary parts of third-order nonlinear susceptibilities (I$m\gamma$), and the transition natures are collected in Table 3. We chose (E)−CpFe(η-C_5H_4)CH═CHC_6H_5 (**A** in Table 3) and Fe-{η-C_5H_4−(E)−CH═CH−4-C_6H_4C≡CH}$_2$ (**B** in Table 3) as examples to examine our calculation method. As shown in Table 3, our calculated results are in good agreement with the experimental values. The maximum TPA positions for **1**−**4**, **5**−**7**, and **8**−**11** are in the ranges 740−760, 860−890, and 650−695 nm, respectively. The maximum TPA of **12** occurs at 792.6 nm. It can be found that the effects of the acceptors on the maximum TPA wavelengths of ferrocenyl derivatives are smaller, while increasing the π-bridge conjugation length leads to large red shifts of the maximum TPA wavelengths (120−140 nm). In comparison with the dipolar molecules, the maximum TPA wavelengths of the quadrupole molecules are blue-shifted by 67−94 nm.

The maximum TPA cross sections increase as the strengths of the acceptors increase. The maximum TPA cross section of

TABLE 3: TPA Properties for Studied Molecules

mol	λ^{T}_{max}/nm	I$m\gamma$/10^{-36} esu	δ_{max}/GM	CI coefficient
1	748.6	4114.15	505.87	−0.32(H−2 → L+12) − 0.56(H−1 → L) + 0.34(H−1 → L+13)
2	742.6	4819.35	605.55	−0.33(H−3 → L) − 0.50(H−2 → L) − 0.34(H−1 → L)
	900.2	2643.98	225.65	0.89(H → L)
3	743.4	5084.19	634.25	0.33(H−3 → L) + 0.50(H−2 → L) − 0.34(H−1 → L)
	897.8	2618.77	225.45	0.89(H → L)
4	760.6	4507.35	538.25	0.33(H−3 → L) − 0.53(H−2 → L) + 0.35(H−2 → L +18)
	932.2	4280.81	340.32	0.87(H → L)
5	868.4	7010.88	640.77	0.55(H−1 → L) + 0.38(H → L+1) − 0.49(H,H → L,L)
6	885.2	7960.59	703.28	−0.36(H−3 → L) − 0.49(H−1 → L) − 0.40(H → L+1) − 0.51(H,H → L,L)
7	878.2	8589.70	771.91	−0.36(H−3 → L) + 0.50(H−1 → L) + 0.39(H → L+1) − 0.50(H,H → L,L)
8	654.8	15021.47	2421.93	−0.55(H−3 → L+1)
9	665	15516.52	2423.11	0.34(H−5 → L+1) + 0.53(H−3 → L+1)
10	671.6	16660.67	2551.78	0.45(H−1,H → L,L+1) − 0.39(H,H → L,L) + 0.34(H,H → L+1,L+1)
11	693.0	14334.86	2055.16	0.56(H−3 → L+1)
12	792.6	27000.75	2968.51	−0.47(H−3 → L) −0.34(H−1 → L+2)
A	615.4 (602)[34]	109.34 (105.3)[34]	19.93	−0.72(H−2 → L)+ 0.44(H → L)
B	801.6 (800)[51]	126.27 (160)[51]	13.56 (50)[51]	−0.41(H−2 → L+13)+ 0.36(H−2 → L+14)

TABLE 4: Linear Optical Parameters for the Maximum TPAs for Studied Molecules

mol	$M_{0k}(x)$ (Debye)	$M_{kn}(x)$ (Debye)	$M_{0n}(x)$ (Debye)	$\Delta\mu_n(x)$ (Debye)	E_{0k} (eV)	E_{0n} (eV)	$[M_{0k}(x)M_{kn}(x)]^2/(E_{0k} - E_{0n}/2)^2\Gamma + [M_{0n}(x)\Delta\mu_{0n}(x)]^2/(E_{0n}/2)^2\Gamma$
1	8.33	5.62	1.73	5.29	2.76	3.31	13137.98 (505.87)
2	8.46	6.58	1.18	5.73	2.75	3.34	18946.70 (605.55)
3	8.60	6.75	1.22	5.62	2.76	3.33	20234.12 (634.25)
4	8.43	5.74	0.04	4.69	2.66	3.26	15826.44 (538.25)
5	10.96	4.77	1.22	0.93	2.36	2.85	22248.38 (640.77)
6	12.05	4.23	1.48	1.69	2.25	2.80	25864.24 (703.28)
7	12.13	4.40	1.53	1.74	2.25	2.82	28828.06 (771.91)
8	11.33	7.62	0.04	3.32	2.87	3.79	56087.56 (2421.93)
9	11.18	7.39	1.20	3.30	2.87	3.73	47956.72 (2423.11)
10	11.79	1.68	0.21	2.15	2.88	3.69	2622.08 (2551.78)
11	12.41	5.48	0.50	5.59	2.81	3.58	31504.30 (2055.16)
12	14.37	1.28	0.01	1.56	2.38	3.13	3584.76 (2968.51)

[a] x denotes the molecular long axis. [b] The values in parentheses are the maximum TPA cross sections.

1 is 505.87 GM (1 GM = 10^{-50} cm^4 s/photon). As the TCF in **1** is substituted with CF_3PhTCF or CNPhTCF, the maximum TPA cross sections of **2** and **3** increase by 100 and 128 GM (605.55 GM for **2** and 634.25 GM for **3**), respectively. The maximum TPA cross section of **4** is reduced to 538.25 GM when the CNCNTCF substitutes for the CF_3PhTCF in **2** or CNPhTCF in **3**. The reason for the reduction is the decrease of the couplings between electronic states caused by replacement of phenyl group. Increasing the π-bridge conjugation length leads to enhancement in the maximum TPA cross sections. The maximum TPA cross section of **5** increases by 134.9 GM relative to **1** (640.77 GM vs 505.87 GM, respectively). On going from **2** to **6**, the maximum TPA cross section increases by 97.7 GM (605.55 GM vs 703.28 GM, respectively). The maximum TPA cross section of **7** increases by 134.8 GM relative to **3** (771.91 GM vs 634.25 GM, respectively). Among studied molecules, the quadrupole molecules have the largest TPA cross sections (2421.93, 2423.11, 2551.78, 2055.16, and 2968.51 GM for **8**−**12**, respectively), which are about 4 times the values of the corresponding dipolar molecules, indicating the stronger interactions between the top and bottom branches.

According to eq 4, the linear optical parameters for the maximum TPAs of the studied molecules are summarized in Table 4. The relationship between δ_{max} and $[M_{0k}(x)M_{kn}(x)]^2/[(E_{0k} - E_{0n}/2)^2\Gamma] + [M_{0n}(x)\Delta\mu_{0n}(x)]^2/[(E_{0n}/2)^2\Gamma]$ for **1**−**7** is plotted in Figure 4. From Table 4 and Figure 4, some important conclusions can be drawn: (1) For the dipolar molecules, the charge transfers mainly occur on the x axis (the molecular long axis), and the positions and relative strengths of the maximum TPAs can be predicted with the three-state formula. As shown in Figure 4, the calculated points are averagely distributed on the two sides of the straight line. (2) The increase in transition dipole moments between the ground states and the intermediate states and the increase in transition dipole moments between the intermediate states and the final states are main reason for enhancement of the maximum TPA cross sections from **1** to **4** to **2** to **3** and from **6** to **7**. The CF_3PhTCF and CNPhTCF with a phenyl group cause larger transition dipole moments than stronger acceptor CNCNTCF. On going from **5** to **6**, the increase of the maximum TPA cross sections is ascribed to a reduction of the energy tuning term $(E_{0k} - E_{0n}/2)$ (0.87 eV vs 0.72 eV, respectively). (3) The increase of the π-bridge conjugation length leads to enhancement of transition dipole moments between the

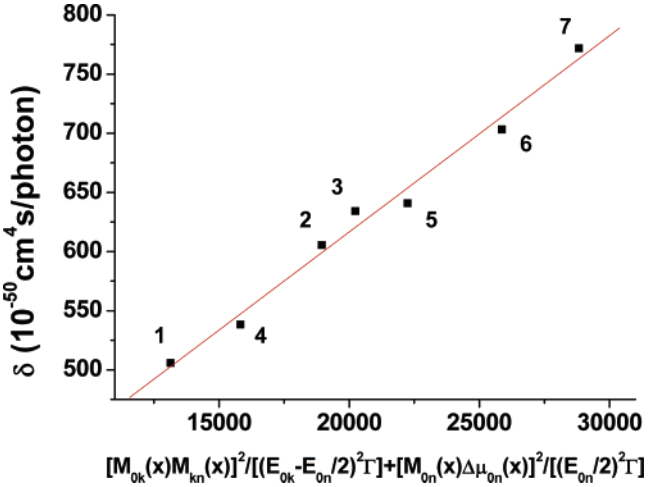

Figure 4. Relationship between δ_{max} and $[M_{0k}(x)M_{kn}(x)]^2/[(E_{0k} - E_{0n}/2)^2\Gamma] + [M_{0n}(x)\Delta\mu_{0n}(x)]^2/[(E_{0n}/2)^2\Gamma]$ for **1**−**7**.

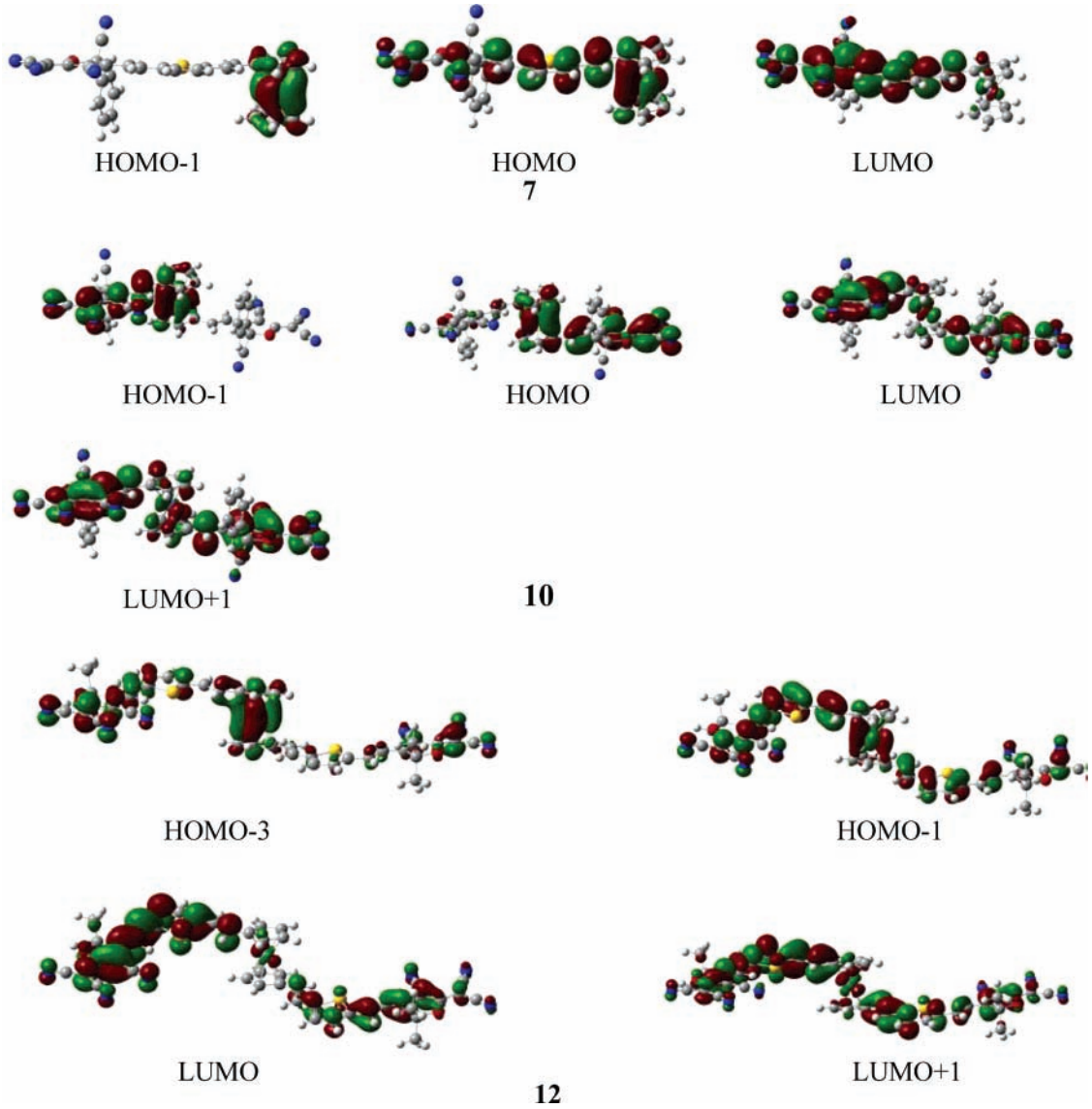

Figure 5. Contour surfaces of the frontier orbitals relevant to TPAs for **7**, **10**, and **12**.

ground states and the intermediate states and reduction of the energy tuning term $(E_{0k} - E_{0n}/2)$, enhancing the TPA cross sections of ferrocenyl derivatives. (4) Analyzing the values of δ_{max} and $[M_{0k}(x)M_{kn}(x)]^2/[(E_{0k} - E_{0n}/2)^2\Gamma] + [M_{0n}(x)\Delta\mu_{0n}(x)]^2/[(E_{0n}/2)^2\Gamma]$, we can find that the TPAs for the quadrupole molecules **8**−**12** do not satisfy the three-state formula, possibly due to stronger interactions between the top and bottom branches. From Table 1 in the Supporting Information, we find that the third-order nonlinear susceptibilities of **11** and **12** are dominated by three and six channels,[52] respectively. In addition, these molecules are not perfectly linear, and transition dipole moments have larger components on the *y* axis. For example, the values of $M_{05}(y)$ for **8**−**12** are −3.85, 4.63, 3.94, 3.29, and 4.37 D, respectively.

Because many applications are related to two-photon (TP) excitation, we take **7**, **10**, and **12** as examples to analyze the origins of TP of ferrocenyl derivatives in this paragraph. The contours of the frontier molecular orbitals relevant to the maximum TPAs of **7**, **10**, and **12** are plotted in Figure 5. From Table 3, we can find that the maximum TPA of **7** mainly originates from the single electronic excitation from HOMO − 1 to LUMO and the double electronic excitation from HOMO to LUMO. As shown in Figure 5, in **7**, the HOMO − 1 and HOMO are mainly distributed on the ferrocenyl moiety and the latter has some contribution from π-bridge, while the LUMO is largely located on the acceptor with some contribution from π-bridge. Thus, the TP excitation of **7** mainly concentrates on the donor (ferrocenyl) moiety to the acceptor (CNPhTCF) part. The maximum TPA of **10** comes from the double electronic excitations from HOMO − 1 and HOMO to LUMO and LUMO + 1, HOMO to LUMO and HOMO to LUMO + 1. In the case of **10**, the HOMO − 1 and HOMO are mainly distributed on the ferrocenyl moiety, and the former has many contributions from the top branch and the latter has some contribution from the bottom branch, while the LUMO and LUMO + 1 are largely located on the acceptor moiety with some contribution from the π-bridge. Apparently, the TP excitation of **10** mainly focuses on the donor (ferrocenyl) moiety to the acceptor (CNPhTCF) moiety. For **12**, the maximum TPA roots in the single electronic excitations from HOMO − 3 to LUMO and HOMO − 1 to LUMO + 2. In **12**, the HOMO − 3 and HOMO − 1 are mainly distributed on the ferrocenyl moiety, and the latter has some contribution from the π-bridge; the LUMO is largely located on the acceptor part with some contribution from the π-bridge, and the LUMO + 2 is mainly distributed on the π-bridge. Thus, the TP excitation of **12** mainly concentrates on the ferrocenyl moiety to the top and bottom two branches. By the analysis of origins of the TP excitations for other ferrocenyl derivatives,

we can obtain the same conclusion that the TP excitations of ferrocenyl derivatives mainly concentrate on the donor (ferrocenyl) moiety to the acceptor part. In other words, the TP excitations of ferrocenyl derivatives originate from the metal-to-ligand transitions (MLCT).

4. Conclusion

In this paper, the electronic structures and one- and two-photon absorption properties of a series of ferrocenyl derivatives with TCF-type acceptors have been studied. First, their equilibrium geometries are optimized at the B3LYP/6-31G level. Then, on the basis of the corrected geometries, the electronic structures and the OPA spectra of the ferrocenyl derivatives have been obtained. Though the ZINDO method less accurately predicts the characteristics of the weak longer-wavelength optical absorptions, it reproduces the intense higher-energy transitions (MLCT). The results show that the higher-energy absorptions are red-shifted as the strengths of acceptors and the π-bridge conjugation length increase. The higher-energy absorptions of the quadrupole molecules are blue-shifted relative to the dipolar molecules, and the absorption intensities are increased by about one time. The TPA properties of the ferrocenyl derivatives have been calculated by using ZINDO−SOS method. The maximum TPA cross sections of the ferrocenyl derivatives increase with increasing strengths of the acceptors and the π-bridge conjugation length. Particularly, the TCF-type acceptor with a phenyl group can lead to the larger TPA cross section. The maximum TPA cross sections of the quadrupole molecules are about 4 times those of the dipolar molecules, indicating the stronger interactions between the top and bottom branches via iron. The TPAs of the quadrupole molecules **8**−**12** do not satisfy the three-state formula, and the possible reasons are discussed. Finally, taking **7**, **10**, and **12** as examples, we discussed the two-photon excitations of the ferrocenyl derivatives and draw a conclusion that the two-photon excitations of ferrocenyl derivatives mainly originate from MLCTs. The quadrupole ferrocenyl derivatives with the TCF-type acceptors have large TPA cross sections (2000−3000 GM) and have good transparency (intense absorptions at 400−520 nm); thus, they are promising candidates for TPA materials.

Acknowledgment. This work is supported by the National Nature Science Foundation of China and the Key Laboratory for Supramolecular Structure and Materials of Jilin University.

Supporting Information Available: Cartesian coordinates for all the optimized geometries for **1**−**12**, **A**, and **B**; selected bond lengths for the ferrocenyl group in the optimized geometries for **1**, **2**, **5**, and **6**, as well as available single-crystal X-ray diffraction data; choice of the number of state basis included in both the configuration interaction and the SOS expansion; contour surfaces of the frontier orbitals relevant to OPA and TPA; transition dipole moments between main electronic states at ZINDO/SDCI level; and main channels for the third-order molecular polarizabilites for **1**−**12**. This material is available free of charge via the Internet at http://pubs.acs.org.

References and Notes

(1) Bhawalkar, J. D.; He, G. S.; Prasad, P. N. *Rep. Prog. Phys.* **1996**, *59*, 1041.

(2) He, G. S.; Zhao, C.-F.; Bhawalkar, J. D.; Prasad, P. N. *Appl. Phys. Lett.* **1995**, *67*, 3703.

(3) Zhao, C.-F.; He, G. S.; Bhawalkar, J. D.; Park, C. K.; Prasad, P. N. *Chem. Mater.* **1995**, *7*, 1979.

(4) Fleitz, P. A.; Sutherland, R. A.; Stroghendl, F. P.; Larson, F. P.; Dalton, L. R. *SPIE Proc.* **1998**, *3472*, 91.

(5) He, G. S.; Bhawalkar, J. D.; Zhao, C.-F.; Prasad, P. N. *Appl. Phys. Lett.* **1995**, *67*, 2433.

(6) Ehrlich, J. E.; Wu, X.-L.; Lee, I.-Y. S.; Hu, Z.-Y.; Röeckel, H.; Marder, S. R.; Perry, J. W. *Opt. Lett.* **1997**, *22*, 1843.

(7) Bhawalkar, J. D.; Kumar, N. D.; Zhao, C.-F.; Prasad, P. N. *J. Clin. Laser Med. Surg.* **1997**, *15*, 201.

(8) Denk, M.; Strickler, J. H.; Webb, W. W. *Science* **1990**, *248*, 73.

(9) Xu, C. M.; Webb, W. W. *Opt. Lett.* **1995**, *20*, 2532.

(10) Wu, E. S.; Stricker, J. H.; Harrell, W. R.; Webb, W. W. *SPIE Proc.* **1992**, *1674*, 776.

(11) Kannan, R.; He, G. S.; Yan, L. X.; Xu, F. M.; Prasas, P. N.; Dombroskie, A. G.; Reinhardt, B. A.; Baur, J. W.; Vaia, R. A.; Tan, L. S. *Chem. Mater.* **2001**, *13*, 1896.

(12) Reinhardt, B. A.; Brott, L. L.; Clarson, S. J. *J. Chem. Mater.* **1998**, *10*, 1863.

(13) Rumi, M.; Ehrlich, J. E.; Heikal, A. A.; Perry, J. W.; Barlow, S.; Hu, Z. Y.; McCord-Maughon, D.; Parker, T. C.; Rockel, H.; Thayumanavan, S.; Marder, S. R.; Beljonne, D.; Breads, J. L. *J. Am. Chem. Soc.* **2000**, *122*, 9500.

(14) Kim, O. K.; Lee, K. S.; Woo, H. Y.; Kim, K. S.; He, G. S.; Swiatkiewicz, J.; Prasad, P. N. *Chem. Mater.* **2000**, *12*, 284.

(15) Albota, M.; Beljonne, D.; Bredas, J. L.; Ehrlich, J. E.; Fu, J. Y.; Heikal, A. A.; Perry, J. W.; Rockel, H.; Rumi, M.; Subramaniam, C.; Webb, W. W.; Wu, I. L.; Xu, C. *Science* **1998**, *281*, 1653.

(16) Kannan, R.; He, G. S.; Lin, T. C.; Prasad, P. N.; Vaia, R. A.; Tan, L. S. *Chem. Mater.* **2004**, *16*, 185.

(17) Chung, S. J.; Kim, K. S.; Lin, T. C.; He, G. S.; Swiatkiewicz, J.; Prasad, P. N. *J. Phys. Chem. B* **1999**, *103*, 10741.

(18) Yan, Y. X.; Tao, X. T.; Sun, Y. H.; Wang, C. K.; Xu, G. B.; Yang, J. X.; Ren, Y.; Zhao, X.; Wu, Y. Z.; Yu, X. O.; Jang, M. H. *J. Mater. Chem.* **2004**, *14*, 2995.

(19) Varnavski, O.; Samuel, I. D. W.; Palsson, L. O.; Beavington, R.; Burn, P. L.; Goodson, T. *J. Chem. Phys.* **2002**, *116*, 8893.

(20) Kogej, T.; Beljonne, D.; Meyers, F.; Perry, J. W.; Marder, S. R.; Bredas, J. L. *Chem. Phys. Lett.* **1998**, *298*, 1.

(21) Bartkowiak, W.; Zaleœny, R.; Leszczynski, J. *Chem. Phys.* **2003**, *287*, 103.

(22) Barzoukas, M.; Blachard-Desce, M. *J. Chem. Phys. B* **2000**, *113*, 3951.

(23) Brasselet. S.; Zyss, J. *J. Opt. Soc. Am. B* **1998**, *15*, 257.

(24) Zyss, J.; Ledoux, I. *Chem. Rev.* **1994**, *94*, 77.

(25) Adronov, A.; Fréchet, J. M. J.; He, G. S.; Kim, K.-S.; Chung, S.-J.; Swiatkiewiez, J.; Prasad, P. N. *Chem. Mater.* **2000**, *12*, 2838.

(26) Varnavski, O.; Leanov, A.; Liu. L.; Takacs, J.; Goodson, T. *J. Phys. Chem. B* **2000**, *104*, 179.

(27) Drobizhev, M.; Karotki, A.; Rebane, A.; Spangler, C. W. *Opt. Lett.* **2001**, *26*, 1081.

(28) Joffre, M.; Yarron, D. Silbey, R.; Zyss, J. *J. Chem. Phys.* **1992**, *97*, 5607.

(29) Lee, W.-H.; Lee, H.; Kim, J.-A.; Choi, J.-H.; Cho, M.; Jeon, S.-J.; Cho, B. R. *J. Am. Chem. Soc.* **2001**, *123*, 10658.

(30) Fuks-Janczarek, I.; Nunzi, J. M.; Sahraoui, B.; Kityk, I. V.; Berdowski, J.; Caminade, A. M.; Majoral, J. P.; Martineau, A. C.; Frere, P.; Roncali, J. *Opt. Commun.* **2002**, *209*, 461.

(31) Liu, X.-J.; Feng, J.-K.; Ren, A. M.; Cheng, H.; Zhou, X. *J. Chem. Phys.* **2004**, *120*, 11493.

(32) Sénéchal, K.; Maury, O.; Bozec, H. L.; Ledoux, I.; Zyss, J. *J. Am. Chem. Soc.* **2002**, *124*, 4560.

(33) Das, S.; Nag, A.; Goswami, D.; Bharadwaj, P. K. *J. Am. Chem. Soc.* **2006**, *128*, 402.

(34) Saswati, G.; Marek, S.; Paras, N. P.; Joseph, J. T. *J. Phys. Chem.* **1990**, *94*, 2847.

(35) Kanis, D. R.; Ratner, M. A.; Marks, T. J. *J. Am. Chem. Soc.* **1992**, *114*, 10338.

(36) Calabrese, J. C.; Cheng, L. T.; Green, J. C.; Marder, S. R.; Tam, W. *J. Am. Chem. Soc.* **1991**, *113*, 7227.

(37) Balavoine, G. G. A.; Daran, J.-C.; Iftime, G.; Lacroix, P. G.; Manoury, E.; Delaire, J. A.; Maltey-Fanton, I.; Nakatani, K.; Di Bella, S. *Organometallics* **1999**, *18*, 21.

(38) Matsuzawa, N.; Seto, J.; Dixon, D. A. *J. Phys. Chem. A* **1997**, *101*, 9391.

(39) Kondo, T.; Horiuchi, S.; Yagi, I.; Ye, S.; Uosaki, K. *J. Am. Chem. Soc.* **1999**, *121*, 391.

(40) Li, G.; Song, Y.; Hou, H.; Li, L.; Fan, Y.; Zhu, Y.; Meng, X.; Mi, L. *Inorg. Chem.* **2003**, *42*, 913.

(41) Barlow, S.; Bunting, H. E.; Ringham, C.; Green, J. C.; Bublitz, G. U.; Boxer, S. G.; Perry, J. W.; Marder, S. R. *J. Am. Chem. Soc.* **1999**, *121*, 3715.

(42) Liao, Y.; Eichinger, B. E.; Firestone, K. A.; Haller, M.; Luo, J.; Kaminsky, W.; Benedict, J. B.; Reid, P. J.; Jen, A. K.-Y.; Dalton, L. R.; Robinson, B. H. *J. Am. Chem. Soc.* **2005**, *127*, 2758.

(43) Alain, V.; Blanchard-Desce, M.; Chen, C.; Marder, S. R.; Fort, A.; Barzoukas, M. *Synth. Met.* **1996**, *81*, 133.

(44) Wright, M. E.; Toplikar, E. G.; Lackritz, H. S.; Kerney, J. T. *Macromolecules* **1994**, *27*, 3016.

(45) Caylor, C. L.; Dobrianow, I.; Kimmr, C.; Thome, R. E.; Zipfel, W.; Webb, W. W. *Phys. Rev. E* **1999**, *59*, 3831.

(46) Orr, B. J.; Ward, J. F. *Mol. Phys.* **1971**, *20*, 513.

(47) Dick, B.; Hochstrasser, R. M.; Trommsdorff, H. P. In *Nonlinear Optical Properties of Organic Molecules and Crystals*; Chemla, D. S., Zyss, J., Eds.; Academic: Orlando, 1987.

(48) Beljonne, D.; Wenseleers, W.; Zojer, E.; Shuai, Z.; Vogel, H.; Pond, S. J. K.; Perry, J. W.; Marder, S. R.; Brédas, J.-L. *Adv. Funct. Mater.* **2002**, *12*, 631.

(49) Anderson, W. P.; Edwards, W. D.; Zerner, M. C. *Inorg. Chem.* **1986**, *25*, 2728.

(50) Frisch, M. J.; Trucks, G. W.; Schlegel, H. B.; Scuseria, G. E.; Robb, M. A.; Cheeseman, J. R.; Montgomery, J. A., Jr.; Vreven, T.; Kudin, K. N.; Burant, J. C.; Millam, J. M.; Iyengar, S. S.; Tomasi, J.; Barone, V.; Mennucci, B.; Cossi, M.; Scalmani, G.; Rega, N.; Petersson, G. A.; Nakatsuji, H.; Hada, M.; Ehara, M.; Toyota, K.; Fukuda, R.; Hasegawa, J.; Ishida, M.; Nakajima, T.; Honda, Y.; Kitao, O.; Nakai, H.; Klene, M.; Li, X.; Knox, J. E.; Hratchian, H. P.; Cross, J. B.; Bakken, V.; Adamo, C.; Jaramillo, J.; Gomperts, R.; Stratmann, R. E.; Yazyev, O.; Austin, A. J.; Cammi, R.; Pomelli, C.; Ochterski, J. W.; Ayala, P. Y.; Morokuma, K.; Voth, G. A.; Salvador, P.; Dannenberg, J. J.; Zakrzewski, V. G.; Dapprich, S.; Daniels, A. D.; Strain, M. C.; Farkas, O.; Malick, D. K.; Rabuck, A. D.; Raghavachari, K.; Foresman, J. B.; Ortiz, J. V.; Cui, Q.; Baboul, A. G.; Clifford, S.; Cioslowski, J.; Stefanov, B. B.; Liu, G.; Liashenko, A.; Piskorz, P.; Komaromi, I.; Martin, R. L.; Fox, D. J.; Keith, T.; Al-Laham, M. A.; Peng, C. Y.; Nanayakkara, A.; Challacombe, M.; Gill, P. M. W.; Johnson, B.; Chen, W.; Wong, M. W.; Gonzalez, C.; Pople, J. A. *Gaussian 03*, revision C.02; Gaussian, Inc.: Wallingford, CT, 2004.

(51) Stephanie, K. H.; Mark, G. H.; Joseph, P. M.; Marie, P. C.; Marek, S.; Barry, L.-D.; Graham, A. H.; Anthony, C. W. *J. Organomet. Chem.* **2003**, *670*, 56.

(52) Beljonne, D.; Cornil, J.; Shuai, Z.; Brédas, J. L.; Rohlfing, F.; Bradley, D. D. C.; Torruellas, W. E.; Ricci, V.; Stegeman, G. I. *J. Chem. Phys.* **1997**, *55*, 1505.